ENHANCED MODEL-FREE PREDICTIVE CONTROL FOR VOLTAGE SOURCE INVERTERS USING AN ADAPTIVE OBSERVER

ZAKARIA LAMMOUCHI[1], CHOUAIB LABIOD[1], KAMEL SRAIRI[2], MOHAMED BENBOUZID[3, 4] *

In this paper, a free model predictive control based on the active vector execution time (AVET-MFPC) using an adaptive observer is proposed for two-level voltage source inverters. The traditional model-free predictive control (MFPC) uses the sampling period to select one voltage vector for all candidate vectors according to the minimizing cost function principle. With the proposed control, two vectors are selected at one sampling period. The first vector is an active vector that uses the execution time of the active vector to select it, while the second one is a zero vector as it is applied after the active vector. The execution time is calculated using the ultra-local model (ULM) equation. In the traditional MFPC, the factor in the ULM is chosen with approximate values ranging between ±50 % of the nominal value. This paper proposes an adaptive sliding mode observer (ASMO) with an improved design to observe the variation of this factor, especially in case of mismatch parameters and during a step change in the reference signal. Combining the proposed ASMO observer and the AVET-MFPC controller gives faster system response, good tracking results, and less computational burden. Finally, the effectiveness of the proposed control model is approved and confirmed under various conditions, as well as the simulations carried out and the results obtained.

1. INTRODUCTION

Various control strategies have been developed in recent years to assist in energy conversion; the predictive control strategies based on the model are one such strategy for controlling voltage source inverters (VSIs); the principle of these strategies is to select the best vector associated with the minimized cost function [1, 2]. To determine the optimal voltage vector, evaluating all vectors, which amount to eight switching states for a two-level inverter, is necessary based on a predictive model [3–5], which requires very precise system parameters [6 ,7]. However, if these parameters contain measurement errors or undergo changes due to varying working conditions, the performance of MPC can be greatly destroyed.

A recent model-free predictive control (MFPC) concept has emerged as an alternative solution for parameter variations in MPC [8]. Within MFPC theory, output derivatives are directly articulated in terms of the input through a ULM. In this theory, online identification techniques must estimate an unknown variable [9]. The traditional MFPC control uses the sampling period to select one voltage vector for the all-candidate [10]. This paper introduces a novel approach termed execution time of active vector-based free model predictive control (AVET-MFPC) tailored for two-level inverters. Two vectors are selected at one sampling period. The first vector is an active vector that uses the execution time of the active vector to select it, while the second is a zero vector as it is applied after the active vector. With the proposed control, there is less computational burden as it uses only six voltage vectors in the cost function instead of all eight candidate vectors. The execution time AVET is calculated using the ULM.

In [11], ULM's extended state observer (ESO) is proposed to simplify AVET-MFPC. In contrast, it finds that the unknown function in ULM has a non-linear character. As discussed in [12], the estimation of the unknown term in the ULM was reached using a sliding mode observer (SMO). Nevertheless, the invariance principle needs to be maintained. Fortunately, this issue can be effectively addressed by using an integral sliding mode observer (ISMO) [13, 14]. The ULM only depends on the two signals, the measured currents and voltage vectors of the system. However, the coefficient multiplied by the input of ULM is related to the system parameters. It is proved in [15, 16] that the factor is chosen with approximate values ranging between ±50 % of the nominal value of the system. This paper proposes an adaptive ISMO observer (AISMO) to observe the unknown function and factor variation in ULM, where this factor is dependent on error current. The factor changes as the current error changes, especially during the initial state and variation load, which leads to a faster response and reduces the resulting current ripple and lower harmonics.

Therefore, this paper deals with the following aspects: section 2 provides a brief overview of the system under study and focuses on the problems of conventional controllers. Section 3 describes details of the proposed AVET-MFPC adaptive controller with AISMO observer to improve the performance system. Section 4 presents the simulation results of the proposed strategy. Finally, section 5 concludes this work.

2. PROBLEM FORMULATION

2.1. PREDICTION MODEL

From Fig. 1, the inverter 2L-VSI has three legs, each containing two switches. The two-level inverter is coupled to an RLE load.
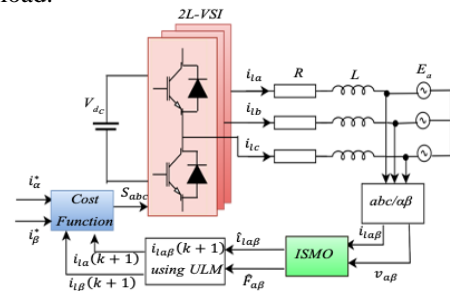
Fig. 1 – Schematic diagram of a 2L-VSI power circuit connected to RLE load for Conventional MFPC.

[1] University of El Oued, Department of Electrical Engineering, El Oued 39000, Algeria
[2] University of Biskra, Department of Electrical Engineering, BP 145, Biskra 07000, Algeria
[3] University of Brest, Institut de Recherche Dupuy de Lôme (UMR CNRS 6027 IRDL), 29238 Brest, France
[4,*] Shanghai Maritime University, Logistics Engineering College, Shanghai 201306, China
Emails: lammouchi-zakaria@univ-eloued.dz, labiod-chouaib@univ-eloued.dz, k.srairi@univ-biskra.dz, mohamed.benbouzid@univ-brest.fr

The connection can simulate a grid-tied PV power generation system [17, 18].

The mathematical representation of the connection is as follows:

$$v_i = Ri_l + L\frac{di_l}{dt} + E \,. \tag{1}$$

The dynamics of equation (1) can be written in the fixed reference frame α-β using the Clark transformation as:

$$\frac{di_{l\alpha}}{dt} = \frac{1}{l}\left(v_{i\alpha} - Ri_{l\alpha} - E_\alpha\right), \tag{2}$$

$$\frac{di_{l\beta}}{dt} = \frac{1}{l}\left(v_{i\beta} - Ri_{l\beta} - E_\beta\right), \tag{3}$$

where $(v_{i\alpha}, v_{i\beta})$ and $(i_{l\alpha}, i_{l\beta})$ are the voltage vector and load current vector components, respectively, in the α-β frame.

The output currents prediction can be formulated using first-order Euler approximation as follows [19]:

$$i_{l\alpha}(k+1) = \frac{T_s}{L}\left(-Ri_{l\alpha}(k) - E_\alpha(k) + v_{i\alpha}(k)\right) + i_{l\alpha}(k), \tag{4}$$

$$i_{l\beta}(k+1) = \frac{T_s}{L}\left(-Ri_{l\beta}(k) - E_\beta(k) + v_{i\beta}(k)\right) + i_{l\beta}(k). \tag{5}$$

The predictive control based on MPC utilizes a mathematical model to predict the future of the output current. Nevertheless, this approach encounters several types of uncertainty, including parameter mismatch. To address the issue of model uncertainty, this paper employs the ULM.

2.2. ULTRA-LOCAL MODEL

To simplify the complexity associated with mathematical models, the concept of an ultra-local model has been incorporated into model-free predictive control theory. The ULM model is defined as [11]:

$$\dot{y} = F + \lambda u, \tag{6}$$

where y and u are the output and input signals for ULM model, respectively, λ denotes the input coefficient. In this context, F is defined as the unknown terms; it consists of the all-diverse type of uncertainty. Generally, a common strategy with MFPC for the online estimation of F is the algebraic identification technique [20].

2.3. MFPC CONTROLLER

Substituting the dynamic equation of system (2) and (3) into the ULM model, the first-order ULM of system can be written as in [21]:

$$\frac{di_{l\alpha}}{dt} = F_\alpha + \lambda v_{i\alpha}, \tag{7}$$

$$\frac{di_{l\beta}}{dt} = F_\beta + \lambda v_{i\beta}. \tag{8}$$

From (7) and (8), the structure of ULM is independent parameters of model. Also, $F_{\alpha,\beta}$ are time-varying unknown functions. In MFPC, the $F_{\alpha,\beta}$ undergoes continuous updates that are determined by utilizing input and output measurements as shown in Fig. 1. According to (7), (8), the derivative current (during sampling period T_s can be expressed using first-order Euler approximation of discrete signal as:

$$\frac{di_l}{dt} \approx \frac{i_l(k+1)-i_l(k)}{T_s} = F_{\alpha,\beta} + \lambda v_{i,A}. \tag{9}$$

The current prediction at $(k+1)$ can be written as:

$$\vec{i}_{l\alpha,\beta}(k+1) = \vec{i}_{l\alpha,\beta}(k) + T_s\left(\vec{F}_{\alpha,\beta} + \lambda\vec{v}_{i,A}\right). \tag{10}$$

The current references utilized in the cost functions are derived at $(k+1)$. It can be estimated using the second order formula of the Lagrange extrapolation as follows:

$$i_\alpha^*(k+1) = 3i_\alpha^*(k) - 3i_\alpha^*(k-1) + 3i_\alpha^*(k-2), \tag{11}$$

$$i_\beta^*(k+1) = 3i_\beta^*(k) - 3i_\beta^*(k-1) + 3i_\beta^*(k-2). \tag{12}$$

The cost function of the MFPC can be writing to obtain optimal vector among the eight feasible ones with a 2-level VSI [1], which directly compares between the reference

vector and candidate vector as:

$$G_{|i=1:8} = \text{abs}\left(i_\alpha^* - i_{l\alpha}(k+1)\right) + \text{abs}\left(i_\beta^* - i_{l\beta}(k+1)\right) \tag{13}$$

From the expression of cost function in (13), the traditional MFPC control uses the sampling period to select one voltage vector from the all-candidate.

Moreover, the algebraic identification technique is an online estimation approach [22] and it was used to estimate $F(\alpha,\beta)$ in real-time [23]. However, conventional MFPC uses complex techniques and more burden-time consuming or classic ISMO observer to estimate the unknown part. In this paper, an adaptive observer AISMO is proposed to estimate the unknown function and observe the variation of the factor in ULM.

3. PROPOSED CONTROL AVET-MFPC WITH AISMO

To improve control performance in terms of reducing the output current ripple signal, reducing the distortion rate, fast response and the robustness of the control in case parameter mismatch. This paper proposed AVET-MFPC with an observer AISMO.

3.1. AVET-MFPC CONTROL

With the proposed control, two vectors are selected at first vector is an active vector that uses the execution time of the active vector to select it, while the second is a zero vector as it is applied after the active vector. The active vector is executed at a one sampling period.

The certain time (t_A), and the zero vectors is enabled at the remaining time (t_Z) of the period to mitigate the changing direction. Thus, a sample period is split up as:

$$T_s = t_A + t_z. \tag{14}$$

Therefore, the one period is spilt into $t(k)$ to $t(k + t_A)$ and $t(k + t_A)$ to $t(k + 1)$, as shown in Fig. 2.

At $t(k+t_A)$, the current predictions $\vec{i}_{l\alpha,\beta}(k + t_A)$ are obtained by directly applying the six feasible vectors $(\vec{v}_{i,A|1\ldots6})$. All other six vectors are shown in Table 1.
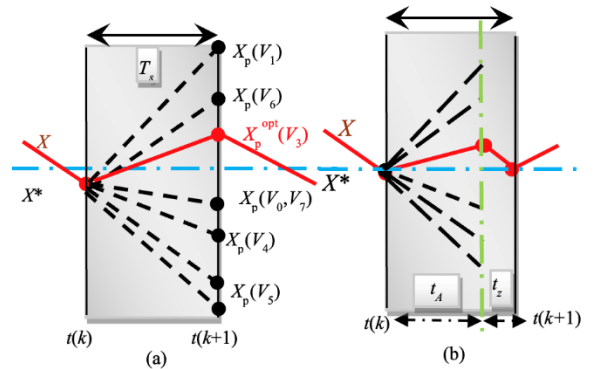
Fig. 2 – Conventional MFPC and proposed AVET-MFPC in one sampling period: a) conventional MFPC; b) AVET- MFPC

Table 1
Six feasible active voltage vectors.

$v_{i,A}$	v_1	v_2	v_3	v_4	v_5	v_6
S_i	100	110	010	011	001	101

According to (7), (8), the derivative current during t_A can be expressed using first-order Euler approximation of discrete signal [19] a:

$$\frac{di_l}{dt} \approx \frac{i_l(k+t_A)-i_l(k)}{t_A} = F_{\alpha,\beta} + \lambda v_{i,A}. \tag{15}$$

The current prediction at $(k + t_a)$ write as:

$$\vec{i}_{l\alpha,\beta}(k + t_A) = \vec{i}_{l\alpha,\beta}(k) + t_A\left(\vec{F}_{\alpha,\beta} + \lambda\vec{v}_{i,A}\right) \quad (16)$$

As shown in Fig. 1, the predicted current at $(k + 1)$ can be obtained by directly applying the zero vectors $(\vec{V}_{s,|7 \text{ or } 8})$ between $t = (k + t_A)$ and $t = (k + 1)$ as:

$$\vec{i}_{l\alpha,\beta}(k + 1) = \vec{i}_{l a\alpha,\beta}(k + t_A) + t_z\left(\vec{F}_{\alpha,\beta} + \lambda\vec{v}_{i,A|7 \text{ or } 8}\right)$$

$$\vec{i}_{l\alpha,\beta}(k + 1) = \vec{i}_{l\alpha,\beta}(k + t_A) + t_z\left(\vec{F}_{\alpha,\beta} + \lambda \cdot 0\right)$$

$$\vec{i}_{l\alpha,\beta}(k + 1) = \vec{i}_{l\alpha,\beta}(k + t_A) + t_z\vec{F}_{\alpha,\beta}. \quad (17)$$

3.2. ACTIVE VECTOR EXECUTION TIME CALCULATION

Combining eq. (16) and (17), one can obtain the execution time of the active vector. The predicted current in $(k+1)$ can be expressed as

$$\vec{i}_{l\alpha,\beta}(k + 1) = \vec{i}_{l-a\alpha,\beta}(k + t_A) + t_z\vec{F}_{\alpha,\beta} =$$

$$= \vec{i}_{l\alpha,\beta}(k) + t_A\left(\vec{F}_{\alpha,\beta} + \lambda\vec{v}_{i,A|1,..6}\right) + t_z\vec{F}_{\alpha,\beta}, \quad (18)$$

where $t_z = T_s - t_A$ and

$$\vec{i}_{l\alpha,\beta}(k + 1) = \vec{i}_{l\alpha,\beta}(k) + t_a\left(\vec{F}_{\alpha,\beta} + \lambda\vec{v}_{i,A|1,..6}\right) +$$

$$+(T_s - t_A)\vec{F}_{\alpha,\beta}.$$

After simplifying,

$$\vec{i}_{l\alpha,\beta}(k + 1) = \vec{i}_{l\alpha,\beta}(k) + t_A\lambda\vec{v}_{i,A|1,..6} + T_s\vec{F}_{\alpha,\beta}. \quad (19)$$

From (19), the execution time of the active vector can be expressed as:

$$t_A = \frac{\vec{i}_{l\alpha,\beta}(k+1) - \vec{i}_{l\alpha,\beta}(k) - T_s\vec{F}_{\alpha,\beta}}{\lambda\vec{v}_{i,A|1,..6}}. \quad (20)$$

Theoretically, by applying two vectors in one period, an active vector at time t_A and a zero vector at t_Z, the output current follows the reference at the time $(k + 1)$ with nearly zero-state errors, so

$$\left\|\begin{matrix} i_{l\alpha}(k + 1) = i_{\alpha}^*, \\ i_{l\beta}(k + 1) = i_{\beta}^*. \end{matrix}\right. \quad (21)$$

Finally, the execution time expression (21) can be rewritten as follows:

$$t_A = \frac{i_{\alpha,\beta}^* - \vec{i}_{l\alpha,\beta}(k) - T_s\vec{F}_{\alpha,\beta}}{\lambda v_{i,A|1,..6}} \quad (22)$$

From (11), (12), and (19), the cost function of the proposed technique can be rewritten to deduce the optimal vector $(k + 1)$ for the six possible active vectors:

$$G_{|i=1:6} = \text{abs}\left(i_{\alpha}^* - i_{l\alpha}(k + 1)\right) + \text{abs}\left(i_{\beta}^* - i_{l\beta}(k + 1)\right). \quad (23)$$

Figure 3 displays the proposed AVET-MFPC control. First, the system's output currents and voltages are measured. Second, the unknown function and the λ factor are estimated using AISMO. This step ensures the optimal value of λ.

In the third step, the execution time of the active vector is calculated using six possible voltage vectors through equation (22). After that, the prediction current and cost function can be obtained according to eq. (19) and (23). Finally, optimal voltages are selected. Then, control [24], as shown in Fig. 3.
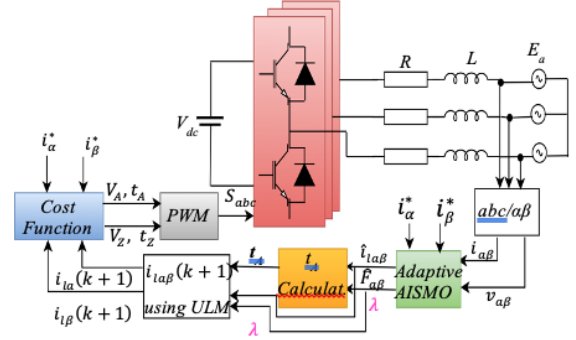
Fig. 3 – Bloc diagram for the proposed control AVET-MFPC.

3.3. MFPC WITH ADAPTIVE ISMO OBSERVER

As presented in [15, 18], the classic design of integral sliding mode observer (ISMO) has been utilized to estimate the unknown function of ULM for the conventional MFPC. This paper proposes an adaptive observer AISMO to observe the unknown function and factor variation in ULM where this factor is dependent on error current. The factor changes as the current error changes, and the proposed observer AISMO is designed as follows:

$$\left|\begin{matrix} e_i = i_l - \hat{\imath}_l, \\ \frac{d\hat{\imath}_l}{dt} = \hat{F}_i + \lambda V_i + u', \\ \frac{d\hat{F}_i}{dt} = e_i + K_i \int_0^t \text{atan}(e_i)\,d\tau, \\ \frac{d\lambda}{dt} = -\delta_1\lambda\left(\delta_2(\lambda - 1) - \frac{\delta_3|e_i^*|}{1+\min(\delta_4,P)}\right), \end{matrix}\right. \quad (24)$$

where e_i is the tracking error, which is the result of the difference between the given desired output $\hat{\imath}_l$ (the estimated current) and the actual output i_l (the actual current) [17]. The coefficients of ISMO, K_i should be chosen as positive values.

To calculate the evaluation of λ, the error e_i^* (*i.e.*, $e_i^* = i^* - \hat{\imath}_l$) is used, where i^* is the reference of the current. The function $P(t)$ represents the power of the output observation error; the following equation gives it:

$$P = \frac{1}{T} \int_{\max(0,t-T)}^t |e_i^*|^2 d\tau. \quad (25)$$

As demonstrated in (24), it is composed of four meticulously selected parameters, namely $\delta_1, \delta_2, \delta_3$ and δ_4. On the other hand, the parameter δ_3 can be assigned high values, primarily intended to saturate the integral term of *P*.

The design of λ in (24) allows the observer gain to take high values, which leads to the paths of the proposed observer converging exponentially and quickly to the trajectory of the system. As a result, the observation error quickly disappears, after which the values of λ decrease to the predetermined value.

3.4. DESIGN OF THE ISMO

The design of the ISMO observer comprises two phases. The first one involves selecting the surface. The control law is formulated in the second phase to ensure that the system tracks converge with the sliding surfaces within a specified time and remain on them. In this paper, the current components are chosen as control variables; note that the integrated sliding mode function for i_α and i_β in the rotating frame is expressed as follows:

$$S_{\alpha\beta} = e_{\alpha\beta} + K_{i\alpha\beta} \int_0^t \text{atan}\left(e_{\alpha\beta}\right)d\tau. \quad (26)$$

From the principle of Lyapunov criterion, it can determine

the input signal u' in (24), and they can be calculated by using the following steps.

To fulfill the stability criterion $\dot{V}_1 < 0$, a Lyapunov function V is defined and chosen as follows:

$$V = \frac{1}{2}\begin{bmatrix} S_\alpha^2 + \hat{e}_{f\alpha}^2 \\ S_\beta^2 + \hat{e}_{f\beta}^2 \end{bmatrix}, \tag{27}$$

where $\hat{e}_{f\alpha}$ and $\hat{e}_{f\beta}$ are the errors can be defined as: $e_{f\alpha} = F_\alpha^* - \hat{F}_\alpha$ and $e_{f\beta} = F_\beta^* - \hat{F}_\beta$, then, this F_α^* and F_β^* are the best estimation of F_α and F_β respectively. The derivative of (27) can be defined as:

$$\dot{V} = \begin{bmatrix} \dot{V}_\alpha \\ \dot{V}_\beta \end{bmatrix} = \begin{bmatrix} S_\alpha \dot{S}_\alpha - \dot{\hat{F}}_\alpha(F_\alpha^* - \hat{F}_\alpha) \\ S_\beta \dot{S}_\beta - \dot{\hat{F}}_\beta(F_\beta^* - \hat{F}_\beta) \end{bmatrix}. \tag{28}$$

The calculation of $\dot{V}_\alpha$ proceeding by using (26) and (28) as

$$\dot{V}_\alpha = S_\alpha \dot{e}_\alpha + S_\alpha K_{i\alpha} \text{atan}(e_\alpha) - \dot{\hat{F}}_\alpha(F_\alpha^* - \hat{F}_\alpha), \tag{29}$$

where $e_\alpha = i_{l\alpha} - \hat{i}_{l\alpha}$, the derivation is used to calculate $\dot{V}_\alpha$

$$\dot{V}_\alpha = S_\alpha\left(\frac{di_{l\alpha}}{dt} - \frac{d\hat{i}_{l\alpha}}{dt}\right) + S_\alpha K_{i\alpha}\text{atan}(e_\alpha) - \dot{\hat{F}}_\alpha(F_\alpha^* - \hat{F}_\alpha). \tag{30}$$

By putting the expression of $\frac{di_{l\alpha}}{dt}$ and $\frac{d\hat{i}_{l\alpha}}{dt}$ as:

$$\dot{V}_\alpha = S_\alpha(F_\alpha + \lambda V_{s\alpha} - \hat{F}_\alpha - \lambda V_{s\alpha} - u'_\alpha) + \\ + S_\alpha K_{i\alpha}\text{atan}(e_\alpha) - \dot{\hat{F}}_\alpha(F_\alpha^* - \hat{F}_\alpha). \tag{31}$$

After simplifying,

$$\dot{V}_\alpha = S_\alpha(F_\alpha - \hat{F}_\alpha) - S_\alpha u'_\alpha + S_\alpha K_{i\alpha}\text{atan}(e_\alpha) - \dot{\hat{F}}_\alpha(F_\alpha^* - \hat{F}_\alpha). \tag{32}$$

We add and subtract the function F_α^* in the first part of (32) and at the same time, substitute $\dot{\hat{F}}_\alpha$ by S_α as in (26). Therefore, (32) turns to:

$$\dot{V}_\alpha = S_\alpha\left(e_{f\alpha} - u'_\alpha + K_{i\alpha}\text{atan}(e_\alpha)\right). \tag{33}$$

Assuming e_{fmax} is the upper bound of e_α, $i.e.$, $|e_{f\alpha}| < e_{fmax}$. The integral sliding mode input signal u'_α is chosen as follows:

$$u'_\alpha = \frac{|S_\alpha|}{S_\alpha}e_{fmax} + K_{i\alpha}\text{atan}(e_\alpha) + S\eta_\alpha\text{atan}(S_\alpha). \tag{34}$$

Finally, from (33) and (34), $\dot{V}_\alpha$ can be rewritten as:

$$\dot{V}_\alpha = S_\alpha e_{f\alpha} - |S_\alpha|e_{fmax} - S_\alpha\eta_d\text{atan}(S_\alpha). \tag{35}$$

Since $-S_\alpha\eta_\alpha\text{atan}(S_\alpha)$ is always negative and $S_\alpha e_{f\alpha} < |S_\alpha|e_{fmax}$, as shown in the previous equations, the derivation of the Lyapunov function is negative, and the stability conditions in eq. (35) ensure that the designed observer is stable. The expression u'_β can be derived by

$$u'_\beta = \frac{|S_\beta|}{S_\beta}e_{fmax} + K_{i\beta}\text{atan}(e_\beta) + S\eta_\beta\text{atan}(S_\beta). \tag{36}$$

3. SIMULATION RESULTS

To evaluate the performance and robustness of the conventional MFPC and proposed AVET-MFPC control, the system parameters utilized in this paper are detailed in Table 2.

Table 2

Simulation parameters

simulation detail	Type and parameters of the system
Inductance value	$L = 12$ mH
Resistance value	$R = 1.5\ \Omega$
sampling time T_s	100 µs
Reference frequency	50 Hz
DC-link voltage	80 V

Using an adaptive observer, simulations were implemented in MATLAB software to validate the proposed AVET-MFPC effect. The simulation duration was configured to 0.15 s, maintaining a constant reference frequency of 50 Hz with a maximum value of current equal to 3 A, as shown in Fig. 4.

The simulation results indicate that the proposed AVET-MFPC exhibits superior steady-state performance under accurate parameter settings compared to the conventional MFPC. Total Harmonic Distortion (THD) for conventional MFPC is approximately 1.55 %, whereas for the proposed control, it is around 0.82 %.

To assess the dynamic performance of both methods, the reference current was increased from 1 A to 3 A at 0.165s, as depicted in Fig. 5. Figure 5a shows the system's dynamic tracking capability using a conventional controller with a slow system transition (1.3 ms) compared to the fast performance of the system using the proposed controller AVET-MFPC (2.8 ms), as shown in Fig. 5b. This fast transition with the proposed controller is due to using an adaptive observer to reduce the error between the two currents.
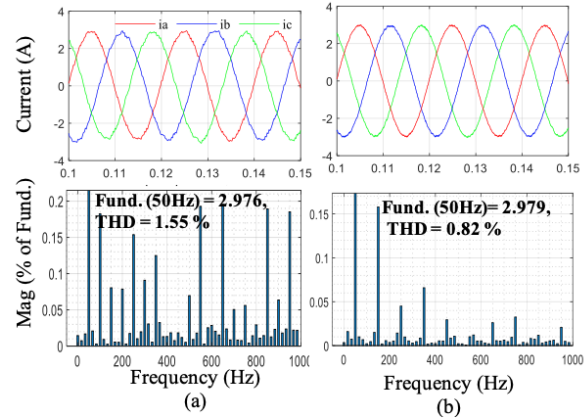
Fig. 4 – Performance of the proposed conventional model-free controller under a peak current reference of 2 A:
a) MFPC; b) AVET-MFPC.

Both controllers effectively track the reference current thereafter. A sensitivity test to the load parameter mismatch was conducted to demonstrate the performance of the AVET-MFPC controller supported by the adaptive observer.
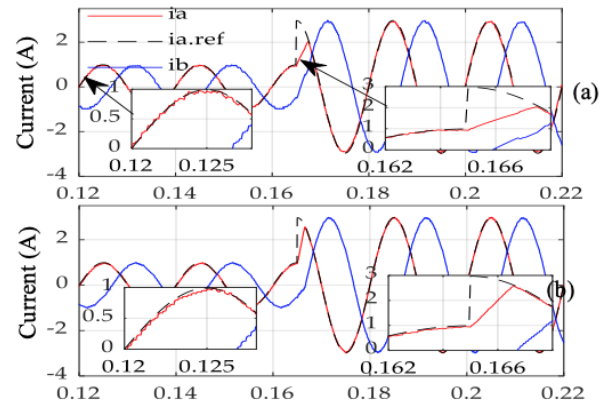
Fig. 5 – Tracking the performance of the conventional and proposed controller during a step-change in the reference current from 1 A to 3 A:
a) MFPC; b) AVET-MFPC.

Figure 6 shows that when the inductance value is changed from L to –30 % L at 0.15 s, the tracking error between the reference and the measured currents increases noticeably

when using the traditional strategy compared to the proposed control. The advantage of the proposed method is that it adapts the factor λ with the AISMO observer in case of mismatch parameters.

4.1. EVALUATE OF FACTOR λ

The input coefficient in the proposed control method, factor λ, is typically considered a nonphysical constant and is often determined through a trial-and-error process. However, in [22], the authors suggested selecting α within the range of ± 50 % of the classical model input coefficient. The output current and the variation of factor λ are displayed in Fig. 7, providing insight into the performance and accuracy of the proposed adaptive observer with MFPC. To evaluate the performance of the Adaptive Observer (AISMO) interconnected with the proposed controller, the reference current is increased from 1 to 3 A, as shown in Fig. 7a, and the second test during the parameter mismatch at 0.15 s is presented in Fig. 7b.
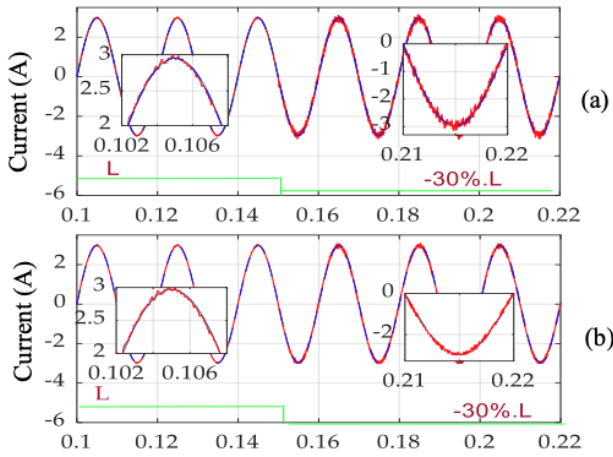
Fig. 6 – Simulation results with variation load: a) the conventional MFPC; b) AVET-MFPC.

Figure 7a presents the dynamic of the factor λ, where it takes on high values when there are convergence errors between the reference and measured currents, especially at the initialization of the tracking, and when the reference current increased from 1 to 3 A at 0.16 s, which leads to faster and better convergence time. After that, the value of λ decreases to a predetermined constant value: nominal value.

From Fig. 7b, a sensitivity test to the load parameter mismatch was conducted to demonstrate the performance of the AVET-MFPC controller supported by the adaptive observer.
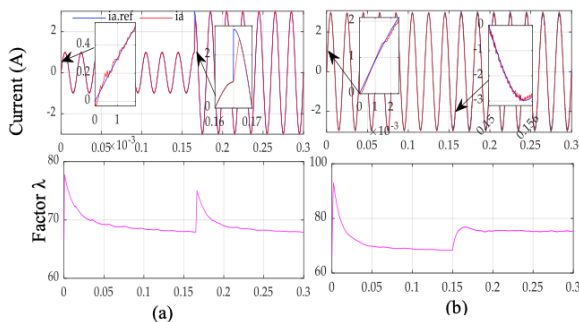
Fig. 7 – Results of λ factor evaluation using adaptive AISMO for AVET-MFPC: a) increased from 1 to 3 A; b) parameter mismatch at 0.15 s.

4.2. SENSITIVITY ANALYSIS

Parameter mismatch testing was conducted in this section

to assess the performance and robustness of the AVET-MFPC proposal.

Figure 8 compares results among three methods: FS-MPC, MFPC, and AVET-MFPC under inductance mismatch by conducting inductance changes ranging from –60 % to + 60 % from nominal inductance. Figure 8 illustrates the test outcomes, which reveal that THDs are impacted by changes in inductance levels for two FS-MPC and MFPC controllers. AVET-MFPC produces output current with a lower THD as its value decreases to 0.82 % when the nominal value of the inductance and THD of 1.13 % with a positive inductance mismatch of 33 mH. The proposed strategy AVET-MFPC showed less impact when there was a mismatch in the inductance value, which showed very good performance compared to the two other strategies.
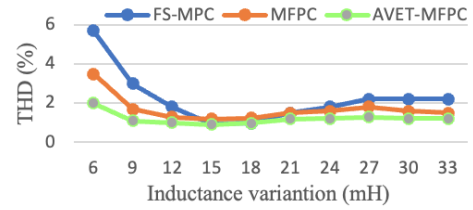
Fig. 8 – Sensitivity of the three techniques FS-MPC, MFPC, and AVET-MFPC to inductance variation.

4.3 PERFORMANCE COMPARISON OF THREE STRATEGIES

Table 3 illustrates a comparison between the three strategies: MPC, MFPC, and AVET-MFPC. AVET-MFPC shows better and faster dynamic tracking performance and complete independence from system parameters. Moreover, the proposed control shows robustness against parameter mismatch.

Table 3

Comparison of three controllers

Strategies	Dynamic performance	System parameters needed	Robustness to parameter mismatch
FS-MPC	Good	*R, L*	Poor
MFPC	**Good**	$\alpha \approx 1/L$	Good
AVET-MFPC	Very Good	Not required	Very Good

5. CONCLUSION

This paper improves free model predictive control by using an adaptive observer. Our approach relies only on the current and voltage of the controlled system and does not require any parameter of the controlled system. To reduce the ripple of the output current, a control technique was used that relies on two vectors, one active and the other zero, during one sampling period. The proposed technique is based on calculating the execution time of the active vector. On the other hand, an adaptive observer was used to get faster response and robustness control in cases of parameter mismatch.

Simulation results confirm better performance compared to conventional MFPC while testing different conditions. Hence, the proposed control has better static and dynamic performances, guaranteeing that the control performance is not affected by parameter mismatch.

The proposed control model can be exploited in systems with complex models, such as motor control or pumping water through photovoltaic systems.

REFERENCES

1. C. Wang, D. Cao, X. Qu, C.Fan, *An improved finite control set model predictive current control for a two-phase hybrid stepper motor fed by a three-phase VSI*, Energies, **15**, *3*, p. 1222 (2022).

2. F. Shiravani, P.Alkorta, J.A. Cortajarena, O. Barambones, *An improved predictive current control for IM drives*, Ain Shams Engineering Journal, **14**, *8*, p. 102037 (2023).

3. M.S. Mousavi, S.A. Davari, V. Nekoukar, C. Garcia, J. Rodriguez, *Model-free finite set predictive voltage control of induction motor*, 12th Power Electronics, Drive Systems, and Technologies Conference (PEDSTC), 2021.

4. M.A. Ilie, D. Floricău, *Grid-connected photovoltaic systems with multilevel converters – modeling and analysis*, Rev. Roum. Sci. Techn.– Électrotechn. et Énerg., **68**, *1*, pp. 77–83 (2023).

5. J. Juan, G. Ignacio, J. Mario, G. Angel, C. Juan, *Guiding the selection of multi-vector model predictive control techniques for multiphase drives,* Machines, **12**, *2*, p. 115 (2024).

6. X. Li, S. Zhang, X. Cui, Y. Wang, C. Zhang, Z. Li, Y. Zhou, *Novel deadbeat predictive current control for PMSM with parameter updating scheme*, IEEE Journal of Emerging and Selected Topics in Power Electronics, **10**, *2*, pp. 2065–2074 (2021).

7. Z. Zhao, P. Davari, Y. Wang, F. Blaabjerg, *Online capacitance monitoring for DC/DC boost converters based on low-sampling-rate approach*, IEEE Journal of Emerging and Selected Topics in Power Electronics, **10**, *5* pp. 5192–5204 (2021).

8. R. Heydari, H. Young, Z. Rafiee, F. Flores-Bahamonde, M. Savaghebi, J. Rodriguez, *Model-free predictive current control of a voltage source inverter based on identification algorithm*, The 46th Annual Conference of the IEEE Industrial Electronics Society (IECON), 2020.

9. W. Huang, Y. Huang, D. Xu, *Model-free predictive current control of five-phase PMSM drives*, Electronics, **12**, *2*, p. 4848 (2023).

10. M. Kermadi, *A Model-Free Predictive Current Controller for Voltage Source Inverters*, Authorea Preprints, 2023.

11. M.S. Mousavi, S.A. Davari, V. Nekoukar, C. Garcia, J. Rodriguez, *Model-free predictive control based on the integral sliding mode observer for induction motor*, 13th Power Electronics, Drive Systems, and Technologies Conference (PEDSTC), IEEE (2022).

12. P.V. Surjagade, S. Shimjith, A. Tiwari, *Second order integral sliding mode observer and controller for a nuclear reactor*, Nuclear Engineering and Technology, **52**, *3*, pp. 552–559 (2020).

13. Z. Zhang, M. Leibold, A. Wollherr, *Integral sliding-mode observer-based disturbance estimation for Euler–Lagrangian systems*, IEEE Transactions on Control Systems Technology, **28**, *6*, pp. 2377–2389 (2019).

14. A. Navid, K. Abbas, *Second order sliding mode control for islanded ac microgrids with renewable power resources*, Rev. Roum. Sci. Techn.– Électrotechn. et Énerg., **69**, *1*, pp. 39–44 (2024).

15. J. Han, *From PID to active disturbance rejection control*, IEEE Transactions on Industrial Electronics, **56**, *3*, pp. 900–906 (2009).

16. M.S. Mousavi, S.A. Davari, V. Nekoukar, C. Garcia, J. Rodriguez, *A robust torque and flux prediction model by a modified disturbance rejection method for finite-set model-predictive control of induction motor*, IEEE Transactions on Power Electronics, **36**, *8*, pp. 9322–9333 (2021).

17. L. Medekhel, M. Hettiri, C.Labiod, K. Srairi, M. Benbouzid, *Enhancing the performance and efficiency of two-level voltage source inverters: a modified model predictive control approach for common-mode voltage suppression*, Energies, **16**, *2*, p. 7305 (2023).

18. Z. Zhang, B. Li, R. Ma, X. Chen, Z. Dai, *Finite control set model predictive control with a constant switching frequency for single-phase grid-connected photovoltaic inverter*, IET Power Electronics, **15**, *2*, pp. 123–131 (2022).

19. B. V. Comarella, D. Carletti, I. Yahyaoui, L.F. Encarnação, *Theoretical and experimental comparative analysis of finite control set model predictive control strategies*, Electronics, **12**, *6*, pp. 1482 (2023).

20. A. Bakeer, G.Magdy, A. Chub, F. Jurado, M. Rihan, *Optimal ultra-local model control integrated with load frequency control of renewable energy sources based microgrids*, Energies, **15**, *2*, p. 9177 (2022).

21. X. Li , Y.Wang, X. Guo, X.Cui, S. Zhang, Y. Li, *An improved model-free current predictive control method for SPMSM drives*, IEEE Access, **9**, pp. 134672–134681 (2021).

22. A. Abid, A. Bakeer, M. Bouzidi, A. Lashab, *Model-free predictive current control for voltage source inverter: a comparative investigation*, International Conference on Electrical Engineering and Advanced Technology (ICEEAT), IEEE, 2023.

23. Y. Wang, H. Li, R. Liu, L. Yang, X. Wang, *Modulated model-free predictive control with minimum switching losses for PMSM drive system*, IEEE Access, **8**, pp. 20942–20953 (2020).

24. Lăudatu, D. Niculae, M. Iordache, M.L. Bobaru, M. Stănculescu, *Experimental analysis of power semiconductor elements used in flyback converters*, Rev. Roum. Sci. Techn.– Électrotechn. et Énerg., **69**, *1*, pp. 67–72 (2024).